Flow and heat transfer over a generalized stretching/shrinking wall problem - exact solutions of the Navier-Stokes equations

Tiegang Fang, Shanshan Yao, Ioan Pop

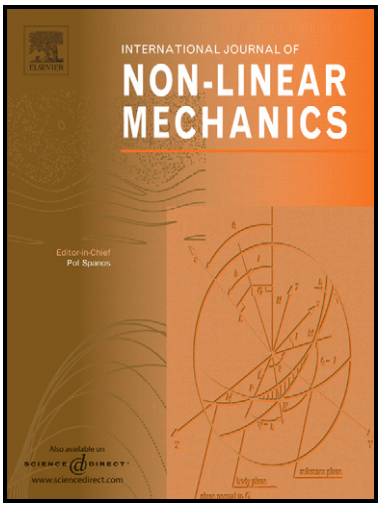

Flow and heat transfer over a generalized stretching/shrinking wall problem - exact solutions of the Navier-Stokes equations

Tiegang Fang, Shanshan Yao, Ioan Pop

PII: S0020-7462(11)00067-9
DOI: doi:10.1016/j.ijnonlinmec.2011.04.014
Reference: NLM 1850

www.elsevier.com/locate/nlm

To appear in: *International Journal of Non-Linear Mechanics*

Received date: 2 November 2009
Accepted date: 5 April 2011

Cite this article as: Tiegang Fang, Shanshan Yao and Ioan Pop, Flow and heat transfer over a generalized stretching/shrinking wall problem - exact solutions of the Navier-Stokes equations, *International Journal of Non-Linear Mechanics*, doi:10.1016/j.ijnonlinmec.2011.04.014

Flow and heat transfer over a generalized stretching/shrinking wall problem - exact solutions of the Navier-Stokes equations

Tiegang Fang and Shanshan Yao
Mechanical and Aerospace Engineering Department
North Carolina State University
3182 Broughton Hall – Campus Box 7910
2601 Stinson Drive
Raleigh, NC 27695

Ioan Pop
Faculty of Mathematics
University of Cluj
R-3400 Cluj
CP 253, Romania

Contact information:
Tiegang Fang: tfang2@ncsu.edu
Ioan Pop: pop.ioan@yahoo.co.uk

Abstract

In this paper, we investigate the steady momentum and heat transfer of a viscous fluid flow over a stretching/shrinking sheet. Exact solutions are presented for the Navier-Stokes equations. The new solutions provide a more general formulation including the linear stretching and shrinking wall problems as well as the asymptotic suction velocity profiles over a moving plate. Interesting nonlinear phenomena are observed in the current results including both exponentially decaying solution and algebraically decaying solution, multiple solutions with infinite number of solutions for the flow field, and velocity overshoot. The energy equation ignoring viscous dissipation is solved exactly and the effects of the mass transfer parameter, the Prandtl number, and the wall stretching/shrinking strength on the temperature profiles and wall heat flux are also presented and discussed. The exact solution of this general flow configuration is a rare case for the Navier-Stokes equation.

Keywords: Navier-Stokes equation; Similarity equation; Stretching surface; Shrinking sheet; Exact solution; Analytical solution; Heat transfer.

1. Introduction

The fluid dynamics over a stretching surface is important in many practical applications, such as extrusion of plastic sheets, paper production, glass blowing, metal spinning, drawing plastic films, the cooling of metallic plates in a cooling bath, polymer sheet extruded continuously from a dye and heat-treated materials that travel between feed and wind-up rolls, to name just a few. Apparently, the quality of the final product depends on the rate of heat and mass transfer between the stretching surface and fluid flow of such processes as explained by Karwe and Jaluria [1]. Since the pioneering study by Crane [2] who presented an exact analytical solution for the steady two-dimensional stretching of a surface in a quiescent fluid with a velocity varying linearly with distance x from a fixed point, many authors have considered various aspects of this problem, such as consideration of mass transfer, power-law variation of the stretching velocity and temperature, magnetic field, application to non-Newtonian fluids, and obtained similarity solutions. Exact solutions for self-similar boundary layer flows induced by a stretching

surface with velocity proportional to x^m, where m is a constant were reported by Banks [3] for an impermeable surface, and by Magyari and Keller [4] for a permeable surface. Liao and Pop [5] solved the case of a linearly stretching surface using the homotopy analytic method (HAM). Carragher and Crane [6], and Grubka and Bobba [7] investigated heat transfer in the above flow in the case when the temperature difference between the surface and the ambient fluid is proportional to a power of distance from the fixed point. Dutta et al. [8] have considered the case of temperature distribution in the flow over a stretching sheet with uniform wall heat flux. Gupta and Gupta [9] analyzed the heat and mass transfer corresponding to the similarity solution for the boundary layers over an isothermal stretching sheet subject to suction or blowing. Bataller [10] performed a numerical analysis in connection with the boundary layer flow and heat transfer of a quiescent fluid over a nonlinearly stretching surface. On the other hand, Magyari and Weidman [11] studied the thermal characteristics of the flow over a semi-infinite flat plate driven by a uniform shear in the far field. Similarity solutions of the thermal and momentum boundary layer flow for a power-law shear driven flow over a semi-infinite flat plate has been reported also by Cossali [12] and Fang [13]. Magyari and Keller [14] presented very interesting results for the boundary layer flow and heat transfer characteristics induced by continuous isothermal surfaces stretched with prescribed skin friction. Andersson [15] has considered the slip-flow of a viscous and incompressible fluid past a linearly stretching sheet. Chakrabarti and Gupta [16], and Pop and Na [17] investigated the flow along a permeable stretching sheet under the effect of a constant transverse magnetic field of a Newtonian fluid, while Anderson et al. [18] considered the case of a power-law fluid, respectively. Quite recently the flow adjacent to a stretching permeable sheet in a Darcy-Brinkman porous medium has been considered by Pantokratoras [19]. Wang [20] analyzed the steady three-dimensional flow of a viscous fluid over a plane surface, which is stretched in its own plane in two perpendicular directions. He also studied the flow caused by the axisymmetric stretching of the surface. Some interesting mathematical results on multiple (dual) solutions for the boundary layer flow over a moving semi-infinite flat plate have been reported by Afzal et al. [21], Afzal [22], Weidman et al. [23], Fang [13] and Ishak et al. [24].

However, little work has been done about the problem of shrinking sheet where the velocity on the boundary is towards a fixed point. Miklavčič and Wang [25] studied the flow over a shrinking sheet with mass flux (suction or injection), which is an exact solution of the Navier-Stokes equations. It has been shown that mass suction is required to maintain the flow over a shrinking sheet. This phenomenon can be found, for example, on a rising and shrinking balloon. This new type of shrinking sheet flow is essentially a backward flow as discussed by Goldstein [26]. Physically, there are two conditions that the flow towards the shrinking sheet is likely to exist: whether an adequate suction on the boundary is imposed (Miklavčič and Wang [25]) suction is required to maintain the flow over a shrinking sheet. Problems of boundary layer flow over shrinking sheets with mass transfer have been studied by Fang [27], Fang et al. [28], Fang and Zhang [29] and Fang et al. [30,31]. Fang [27] considered the flow over a continuously shrinking sheet with a power-law surface velocity and mass transfer. The similarity equations with a controlling parameter $\beta = 2m/(m+1)$ were obtained and solved numerically. Exact solutions were derived for $\beta = -1$ and $\beta = -2$, and also for the power-law index $m = -1$. The stagnation flow over a shrinking sheet was investigated by Wang [32]. Finally, we mention the papers by Hayat et al. [33] on the magnetohydrodynamic and rotating flow over a permeable shrinking sheet and by Lok et al. [34] on the MHD stagnation-point flow towards a shrinking sheet.

Motivated by the above-mentioned investigations and applications, we investigate in this present paper, the behavior of the steady boundary layer flow and heat transfer of a viscous and incompressible fluid towards a permeable (with mass flux) shrinking sheet in a quiescent fluid. The sheet shrinking velocity is $u = u_w(x)$ and the constant wall mass suction velocity is $v = v_w$, which will be specified later. The partial differential equations in two variables are transformed into ordinary differential equations and are solved both analytically and numerically for some values of the physically governing parameters.

2. Basic equations and exact solutions

Consider the steady two-dimensional flow of a viscous and incompressible fluid on a continuously stretching or shrinking sheet with mass transfer in a stationary fluid. It

is assumed that the velocity of the stretching sheet is $u_w(x) = bx + C$, where $b > 0$ is the stretching rate and $b < 0$ is the shrinking rate, respectively, and C is a constant velocity component. It is also assumed that constant mass transfer velocity is v_w with $v_w < 0$ for suction and $v_w > 0$ for injection, respectively. The sheet surface temperature is kept constant at T_w and the ambient fluid temperature is a constant at T_∞. The $x-$axis is measured along the stretching surface and the $y-$axis is perpendicular to it. Under these assumptions the basic steady equations of this problem can be written as

$$\frac{\partial u}{\partial x} + \frac{\partial v}{\partial y} = 0 \tag{1}$$

$$u\,\frac{\partial u}{\partial x} + v\,\frac{\partial u}{\partial y} = -\frac{1}{\rho}\,\frac{\partial p}{\partial x} + \upsilon\,\nabla^2 u \tag{2}$$

$$u\,\frac{\partial v}{\partial x} + v\,\frac{\partial v}{\partial y} = -\frac{1}{\rho}\,\frac{\partial p}{\partial y} + \upsilon\nabla^2 v \tag{3}$$

$$u\,\frac{\partial T}{\partial x} + v\,\frac{\partial T}{\partial y} = \sigma\nabla^2 T \tag{4}$$

where u and v are the velocity components along the $x-$ and $y-$ axes, p is the pressure, ρ is the density, υ is the kinematic viscosity of the fluid, σ is the thermal diffusivity of the fluid, and T is the fluid temperature. In the above energy equation, the viscous dissipation term is neglected. The boundary conditions of these equations are

$$\begin{aligned} &u = u_w(x) = bx + C, \quad v = v_w, \quad T = T_w \quad \text{at} \quad y = 0 \\ &u = 0, \quad T = T_\infty, \quad \text{as} \quad y \to \infty \end{aligned} \tag{5}$$

We assume that Eqs. (1) to (4) subject to the boundary conditions (5) admit the similarity solutions,

$$u = a\,x\,f'(\eta) + C\,g(\eta), \quad v = -\sqrt{a\upsilon}\,f(\eta), \quad T - T_\infty = \theta(\eta)(T_w - T_\infty), \quad \eta = y\sqrt{a/\upsilon} \tag{6}$$

where primes denote differentiation with respect to η with a being a positive constant. We also denote $u_r(x) = ax$ as a reference velocity for this problem and $u = u_r(x)\,f'(\eta) + C\,g(\eta)$. Using Eq. (3) and the boundary conditions (5), we obtain the following expression for the pressure p

$$p = p_0 - \rho\frac{v^2}{2} + \rho\upsilon\frac{dv}{dy} \tag{7}$$

where p_0 is the stagnation pressure. Substituting (6) and (7) into Eqs. (2) and (4), we get the following ordinary differential equations

$$f''' + f f'' - f'^2 = 0 \tag{8}$$

$$g'' + f g' - f' g = 0 \tag{9}$$

$$\theta'' + \Pr f \theta' = 0 \tag{10}$$

subject to the boundary conditions

$$\begin{aligned} &f(0) = s, \quad f'(0) = b/a = \alpha, \quad g(0) = 1, \quad \theta(0) = 1 \\ &f'(\infty) = 0, \quad g(\infty) = 0, \quad \theta(\infty) = 0 \end{aligned} \tag{11}$$

Where s is the mass transfer parameter with $s > 0$ for mass suction and $s < 0$ for mass injection, respectively. Also $\alpha > 0$ is the stretching parameter and $\alpha < 0$ is the shrinking parameter, respectively. Pr is the Prandtl number of the fluid with $\Pr = \upsilon/\sigma$.

A physical quantity of interest is the skin friction coefficient C_f which is defined as

$$C_f = \frac{\tau_w}{\rho u_r^2} \tag{12}$$

where τ_w is the skin friction or shear stress and is given by

$$\tau_w = \mu\left(\frac{\partial u}{\partial y}\right)_{y=0} \tag{13}$$

Using the similarity variables (6), we obtain

$$\mathrm{Re}_x^{1/2} C_f = f''(0) + \frac{C}{u_r} g'(0) \tag{14}$$

where $\mathrm{Re}_x = u_r x/\upsilon$ is the local Reynolds number.

For this flow, the normalized streamlines $\tilde{\psi}$ can be defined as

$$\tilde{\psi} = x f(\eta) + \frac{C}{a}\int_0^\eta g(s)\,ds \tag{15}$$

where $\widetilde{\psi} = \psi/(a\upsilon)^{1/2}$ with ψ defined in the usual way as $u = \partial\psi/\partial z$ and $w = -\partial\psi/\partial x$.

There exists an exact solution for Eq. (8) together with the boundary conditions (11) as follows:

$$f(\eta) = \beta + (s-\beta)e^{-\beta\eta} = \beta - \frac{\alpha}{\beta}e^{-\beta\eta} \tag{16}$$

and

$$f'(\eta) = -\beta(s-\beta)e^{-\beta\eta} = \alpha e^{-\beta\eta}. \tag{17}$$

with

$$\beta = \frac{s \pm \sqrt{s^2 + 4\alpha}}{2}. \tag{18}$$

Then Eq. (9) becomes

$$g'' + [\beta + (s-\beta)e^{-\beta\eta}]g' + \beta(s-\beta)e^{-\beta\eta}\, g = 0 \tag{19}$$

There is a special solution for $g(\eta) = f'(\eta) = \alpha e^{-\beta\eta}$. The general solution for Eq. (19) reads

$$g(\eta) = Ae^{-\beta\eta} + B\{-e^{\frac{(s-\beta)e^{-\beta\eta}}{\beta}} + \frac{e^{-\beta\eta}Ei[\frac{(s-\beta)e^{-\beta\eta}}{\beta}]}{\beta}\} \tag{20}$$

where $Ei(x) = -\int_{-x}^{\infty}\frac{e^{-t}}{t}dt$ is the Exponential integral function, and A and B are two integration constants. Since it requires that $g(\eta) \to 0$ as $\eta \to \infty$. It is obtained $B = 0$ and $A = 1$. Thus the solution of $g(\eta)$ becomes

$$g(\eta) = e^{-\beta\eta}. \tag{21}$$

Therefore the velocity fields become

$$u = b\,x\,e^{-\beta\eta} + C\,e^{-\beta\eta} \tag{22}$$

and

$$v = -\sqrt{a\upsilon}[\beta + (s-\beta)e^{-\beta\eta}]. \tag{23}$$

The non-dimensional stream function becomes

$$\tilde{\psi} = x f(\eta) + \frac{C}{a}\int_0^{\eta} g(s)\,ds = \beta x + x(s-\beta)e^{-\beta\eta} - \frac{C}{a\beta}e^{-\beta\eta}. \qquad (24)$$

Further scrutiny of the momentum equation yields an algebraically decaying solution as

$$f(\eta) = \frac{6}{\eta + \sqrt{-6/\alpha}} \text{ and } f'(\eta) = -\frac{6}{(\eta + \sqrt{-6/\alpha})^2}. \qquad (25a, 25b)$$

It is seen that the algebraically decaying function only exists for a shrinking sheet with $\alpha < 0$. Then the mass suction at the sheet is

$$f(0) = s = \sqrt{-6\alpha}. \qquad (26)$$

Accordingly, Eq. (9) becomes

$$g'' + \frac{6}{\eta + \sqrt{-6/\alpha}}g' + \frac{6}{(\eta + \sqrt{-6/\alpha})^2}g = 0. \qquad (27)$$

There is a general solution for Eq. (27) as

$$g(\eta) = \frac{C_1}{(\eta + \sqrt{-6/\alpha})^2} + \frac{C_2}{(\eta + \sqrt{-6/\alpha})^3}. \qquad (28)$$

Applying the boundary conditions (11) for $g(\eta)$ yields

$$g(\eta) = \frac{C_1}{(\eta + \sqrt{-6/\alpha})^2} + \frac{(-6/\alpha)^{3/2} - C_1\sqrt{-6/\alpha}}{(\eta + \sqrt{-6/\alpha})^3}. \qquad (29)$$

where C_1 is a free parameter, which means there are infinite number of solutions for $g(\eta)$ for a given value of α and the solution is an algebraically decaying function. Then the velocity fields are given as

$$u = b x \frac{-6/\alpha}{(\eta + \sqrt{-6/\alpha})^2} + C\left[\frac{C_1}{(\eta + \sqrt{-6/\alpha})^2} + \frac{(-6/\alpha)^{3/2} - C_1\sqrt{-6/\alpha}}{(\eta + \sqrt{-6/\alpha})^3}\right] \qquad (30)$$

and

$$v = -\sqrt{a\upsilon}\,\frac{6}{\eta + \sqrt{-6/\alpha}}. \qquad (31)$$

The non-dimensional stream function for the algebraically decaying case becomes

$$\tilde{\psi} = x f(\eta) + \frac{C}{a}\int_0^{\eta} g(s)\,ds = \frac{6x}{\eta + \sqrt{-6/\alpha}} - \frac{C}{a}\left[\frac{C_1}{\eta + \sqrt{-6/\alpha}} + \frac{(-6/\alpha)^{3/2} - C_1\sqrt{-6/\alpha}}{2(\eta + \sqrt{-6/\alpha})^2}\right]$$

(32)

The energy equation (10) can be solved by direct integration as

$$\theta(\eta) = 1 - \frac{\int_0^{\eta} e^{-\Pr\beta t - \frac{\Pr\alpha}{\beta^2}e^{-\beta t}} dt}{\int_0^{\infty} e^{-\Pr\beta t - \frac{\Pr\alpha}{\beta^2}e^{-\beta t}} dt}. \tag{33}$$

The heat transfer rate at the wall is related to the temperature gradient at the wall as

$$q_w = -k\left(\frac{\partial T}{\partial y}\right)_{y=0} = -k(T_w - T_\infty)\sqrt{a/\upsilon}\theta'(0). \tag{34}$$

We can obtain

$$-\theta'(0) = \frac{e^{-\frac{\Pr\alpha}{\beta^2}}}{\int_0^{\infty} e^{-\Pr\beta t - \frac{\Pr\alpha}{\beta^2}e^{-\beta t}} dt}. \tag{35}$$

The definite integral in the denominator can be expressed explicitly as follows,

$$\int_0^{\infty} e^{-\Pr\beta t + \frac{\Pr(s-\beta)}{\beta}e^{-\beta t}} dt = \frac{(\frac{\Pr\alpha}{\beta^2})^{-\Pr}}{\beta}\left(\Gamma(\Pr,0) - \Gamma(\Pr,\frac{\Pr\alpha}{\beta^2})\right) \tag{36}$$

where $\Gamma(a,x)$ is the incomplete Gamma function. However, the above solutions for energy equation pose some difficulty in finding explicit integration for the temperature distribution. Another approach to the solution can be conducted using a variable transformation technique. In order to solve this equation, a new variable as $\varepsilon = \Pr\frac{e^{-\beta\eta}}{\beta^2}$ is introduced and substituting it to Eq. (10) yields

$$\varepsilon\frac{d^2\theta}{d\varepsilon^2} + (1 - \Pr + \alpha\varepsilon)\frac{d\theta}{d\varepsilon} = 0 \tag{37}$$

with the boundary conditions as

$$\theta(\Pr/\beta^2) = 1 \quad \text{and} \quad \theta(0) = 0. \tag{38a, 38b}$$

The solution for Eq. (37) reads

$$\theta(\varepsilon) = \frac{\Gamma(\Pr,0) - \Gamma(\Pr,\alpha\varepsilon)}{\Gamma(\Pr,0) - \Gamma(\Pr,\frac{\Pr\alpha}{\beta^2})}. \tag{39}$$

Then the temperature solution becomes

$$\theta(\eta)=\frac{\Gamma(\mathrm{Pr},0)-\Gamma(\mathrm{Pr},\alpha\,\mathrm{Pr}\,\frac{e^{-\beta\eta}}{\beta^2})}{\Gamma(\mathrm{Pr},0)-\Gamma(\mathrm{Pr},\frac{\mathrm{Pr}\,\alpha}{\beta^2})}. \tag{40}$$

This solution is consistent with the previous results for $\alpha=-1$ [35]. The first derivative of $\theta(\eta)$ with respect to η becomes

$$\theta'(\eta)=-\frac{\beta e^{-\frac{\mathrm{Pr}\alpha}{\beta^2}e^{-\beta\eta}}\left(\frac{\mathrm{Pr}\,\alpha}{\beta^2}e^{-\beta\eta}\right)^{\mathrm{Pr}}}{\Gamma(\mathrm{Pr},0)-\Gamma(\mathrm{Pr},\frac{\mathrm{Pr}\,\alpha}{\beta^2})}. \tag{41}$$

Then the heat transfer flux at the wall is given as

$$-\theta'(0)=\frac{\beta e^{-\frac{\mathrm{Pr}\alpha}{\beta^2}}\left(\frac{\mathrm{Pr}\,\alpha}{\beta^2}\right)^{\mathrm{Pr}}}{\Gamma(\mathrm{Pr},0)-\Gamma(\mathrm{Pr},\frac{\mathrm{Pr}\,\alpha}{\beta^2})}. \tag{42}$$

Equation (42) is equivalent to Eq. (35), which further proves the used approach is correct. For the algebraically decaying solution, the energy equation becomes

$$\theta''+\mathrm{Pr}\,\frac{6}{\eta+\sqrt{-6/\alpha}}\theta'=0. \tag{43}$$

The solution can be found as follows,

$$\theta(\eta)=\frac{(\sqrt{-6/\alpha})^{6\mathrm{Pr}-1}}{(\eta+\sqrt{-6/\alpha})^{6\mathrm{Pr}-1}}. \tag{44}$$

In order to match the BC at $\eta\to\infty$, it is required that $\mathrm{Pr}>1/6$. The heat flux at the wall reads

$$-\theta'(\eta)=\frac{6\,\mathrm{Pr}-1}{\sqrt{-6/\alpha}}. \tag{45}$$

3. Results and discussion

The exact solution in this work provides a general formulation for both the stretching sheet (Crane problem [2]) and the shrinking sheet (Miklavčič and Wang problem [25]). In addition, the current results extend the sheet velocity from a pure linear velocity to a more general condition with a constant wall translating velocity. In the

current results, C can be either positive or negative. Therefore, the sheet motion can be shrinking in a certain range of distance from the slot then change to a stretching one or to the opposite. For the current constant wall and ambient temperature conditions, the temperature field does not depend on the horizontal velocity component and only be determined by the vertical velocity field. Also the results offer a type of exact solutions of the full 2-D Navier-Stokes equations, which is rare in the literature. In the following section, some examples will be presented and results will be discussed to show the effects of different parameters on the fluid flow and heat transfer characteristics.

3.1 Momentum equation solution

For the momentum equation, the velocity fields are mainly determined by the mass transfer parameter, *s*, and the wall stretching/shrinking parameter, α. For a given combination of *s* and α, the solution is given by Eq. (18). In order to have a physical finite velocity, the value of β must be positive. Thus it is found that there is one positive root of β for $\alpha > 0$ and two positive roots of β for $\alpha < 0$. For $\alpha = 0$, there is no fluid motion in the x-direction due to the linear sheet motion and $\beta = s$ for $s \geq 0$ and $\beta = 0$ for $s < 0$. In either case, we obtain $f(\eta) = s$ and there is only one velocity component in the $y-$direction. However, due to the constant velocity component, there exists an asymptotic suction velocity profile over a moving plate as follows,

$$u = C e^{-s\eta}. \tag{46}$$

It is also seen that there is no asymptotic solution for mass injection. Based on this finding, it is concluded that *the current exact solution provide a general flow solution for the 2-D Navier-Stokes equations by integrating the stretching/shrinking plate and the asymptotic suction solutions*.

Solution domains of β for different α as a function of *s* are shown in Fig. 1. It is clear there are more than one solution for $\alpha < 0$ and solutions only exist for mass suction with $s \geq \sqrt{-4\alpha}$. The solution domain moves towards a large mass suction for a stronger shrinking rate (smaller values of α). For a given negative value of α, the upper branch solution ("+" sign in Eq. (18)) results in a lager value of β with increasing mass suction parameter. However, for the lower branch solution ("-" sign in Eq. (18)), the value of β

decreases with the increase of mass suction parameter. For a positive value of α, there is only one solution and solution exists for both mass suction and mass injection. The value of β increases with the increase of mass suction parameter α. The value of β directly determines the penetration distance of velocity into the fluid. The boundary layer thickness for the wall stretching/shrinking problem can be defined as the distance from the wall at which the velocity is 1% of the wall velocity. Then it is obtained

$$\eta_{0.01} = \ln(100)/\beta = 4.6052/\beta. \tag{47}$$

The boundary layer thickness is inversely proportional to the value of β. In addition, for a given value of mass suction, the upper branch solution of β decreases with the decrease of a negative α, which means stronger shrinking rate at the sheet. But for the lower solution branch, β decreases with the increase of a negative α. When $\alpha < -s^2/4$, there is no solution for the given flow under similarity form. At the critical value of α with one solution, the value of β is given by $\beta = s/2 = \sqrt{-\alpha}$. Another special case is for an impermeable wall with $s = 0$. For this case, $\beta = \sqrt{\alpha}$ and there is only similar solution for the stretching problem. It is worth mentioning at this end that as in similar physical situations, we postulate that the upper branch solutions are physically stable and occur in practice, whilst the lower branch solutions are not physically obtained. This postulate can be verified by performing a stability analysis but this is beyond the scope of the present paper.

To illustrate the effects of the stretching/shrinking parameters on the velocity fields, some velocity profiles are shown in Figs. 2 and 3. As seen in Fig. 2(a) for the upper solution branch, the value of α changes from 0.5 to the one solution value for $s = 4.0$, namely $\alpha = -4$. It is found the velocity profiles penetrate deeper into the fluid for a smaller value of α. However, the lower solution branch is quite different from the upper solution branch, where velocity penetrates deeper for a larger value of α. There exists crossover points among the velocity profiles for different values of α for the lower solution branch under shrinking conditions, namely $\alpha < 0$. In addition, the upper solution branch has much shorter velocity penetration than the lower solution branch for the same values of s and α. For the stretching sheet problem as shown in Figs. 3(a) and 3(b), solutions exist for both mass suction and mass injection. Under mass suction conditions,

the velocity penetration is quite short and the effects of α on the penetration distance are not so obvious. However, based on Eq. (28), under certain mass suction, the penetration distance becomes shorter for a larger value of positive α. But under certain mass injection, the penetration distance becomes obviously shorter for a larger value of positive α. There are cross-over points among the velocity profiles.

In order to show the flow patterns, examples of dimensionless stream functions are plotted in Figs.4 and 5 for different mass transfer and stretching/shrinking parameters as well as $C/a/\beta$. Without loss of generality, we set $\sqrt{a/\upsilon}$ to be one with $\eta = y$. The streamlines for wall shrinking problem are shown in Figs. 4(a)-4(d) for different solution branches. For the shrinking sheet problem, with a negative value of $C/a/\beta$, the fluid is stretched toward the slot for both solution branches. However, for a positive value of $C/a/\beta$, the sheet is first stretched out of the slot and then it moves toward the slot after a certain distance from the slot. There is a point with $u = 0$ on the sheet for both solution branches at $x = C/b = C/(a\alpha) = (\beta/\alpha)(\frac{C}{a\beta})$. For the stretching sheet problem, as shown in Figs. 5(a)-5(d) for different combinations of parameters, the flow patterns are quite different for mass injection and mass suction. Under mass suction, there exists a point for $u = 0$ with a combination of a positive α and a negative $C/a/\beta$. The fluid is first stretched towards the slot and the stretched away from the slot after passing that point. The fluid is always stretched away from the slot when both α and $C/a/\beta$ are positive. When mass injection is applied at the wall, the vertical velocity becomes zero at a certain distance from the wall with $\eta_{v=0} = \frac{\ln(1+|s|/\beta)}{\beta}$. Again for such a condition, the fluid is always moving away from the slot when both α and $C/a/\beta$ are positive. Interesting flow pattern is observed for the stretching sheet with a negative value of $C/a/\beta$ under mass injection as shown in Fig. 5(d). There exists a saddle point for this condition with both $u = 0$ and $v = 0$ at $x = -C/b = -C/(a\alpha) = -(\beta/\alpha)(\frac{C}{a\beta})$ and $\eta_{v=0} = \frac{\ln(1+|s|/\beta)}{\beta}$.

The algebraically decaying solution is quite different from the exponentially decaying solution. In this part, some examples of the algebraically decaying solution will be presented. As shown in Figs. 6(a) and 6(b) for the plot of $f(\eta)$ and $f'(\eta)$, it is seen the velocity profiles have quite deep flow penetration to the ambient fluid. Interesting observations are found for the flow due to constant velocity component at the wall for function $g(\eta)$. Based on Eq. (29), when $C_1 = 0$, the solution reduces to a very simple form,

$$g(\eta) = \frac{(-6/\alpha)^{3/2}}{(\eta + \sqrt{-6/\alpha})^3} \tag{48}$$

and for $C_1 = -6/\alpha$, it becomes

$$g(\eta) = \frac{-6/\alpha}{(\eta + \sqrt{-6/\alpha})^2}. \tag{49}$$

For other arbitrary values of C_1, the profiles of $g(\eta)$ can be quite complicated. To illustrate this, some plots for different values of C_1 and α are shown in Figs. 7 and 8. In Fig. 7, the plots show the effects of positive C_1 and α on the velocity profiles. One interesting findings is the velocity overshoot near the wall. The overshoot velocity becomes more obvious and larger for a larger value of positive C_1 and $|\alpha|$. However, for a negative C_1 as shown in Figs. 8(a) and 8(b), there also exists velocity overshoot to the negative direction with reversal flows in the boundary layer. These kinds of flow behaviors have not been observed in previous publications for the algebraically decaying solutions. In order to further analyze the variation characteristics of the profile, the first derivative of $g(\eta)$ can be obtained as

$$g'(\eta) = \frac{-2C_1}{(\eta + \sqrt{-6/\alpha})^3} - 3\frac{(-6/\alpha)^{3/2} - C_1\sqrt{-6/\alpha}}{(\eta + \sqrt{-6/\alpha})^4}. \tag{50}$$

By setting $g'(\eta)$ zero, we can get the local extreme value (EV) as

$$g_{EV} = \frac{4C_1^3}{27[(-6/\alpha)^{3/2} - C_1\sqrt{-6/\alpha}]^2}. \tag{51}$$

Then it is seen that there might exist a positive velocity overshoot for a positive value of C_1 and a negative velocity overshoot for a negative value of C_1. Some typical

streamlines for the algebraically decaying flow fields in Figs. 9(a) and 9(b) for a positive value of C/a and a negative value of C/a respectively. Again, in the plots, it is assumed $\sqrt{a/\upsilon}=1$. It is obvious that there is certain point with zero velocity at the wall for a positive value of C/a. It is also seen that the variation of C_1 does not affect the flow pattern near the wall, while the flow field far away from the wall is greatly influenced.

3.2 Heat transfer solution

Now let's look at the heat transfer problem. The dimensionless temperature and heat transfer flux at the wall are given by Eqs. (40) and (42) for exponentially decaying flow and given by Eqs. (44) and (45) for the algebraically decaying flow. In order to illustrate the temperature distribution and heat flux at the wall under the effects of different combinations of mass suction parameter, stretching parameter, and Prandtl number, some typical examples will be presented and discussed in this section.

The effects of the Prandtl number on the temperature profiles are shown in Figs. 10 and 11. The non-dimensional temperature profiles for a shrinking sheet configuration with $\alpha=-2$ and $s=4$ are shown in Figs. 10(a) and 10(b) for the two solution branches at different values of Prandtl number. Generally, the thermal boundary layer thickness becomes thinner with the increase of the Prandtl number. Compared with the upper solution branch, the lower solution branch has slightly thicker thermal boundary layer. For the stretching wall problem with mass suction as shown in Fig. 11(a), the thermal boundary layers are quite similar to the shrinking problem with the same wall motion and mass suction as seen in Fig. 10(a). However, the mass injection case provides very different results (Fig. 11-b). Under mass injection, the boundary layer is blown away from the wall and the heat flux at the wall becomes very small. The boundary layer thickness is still thinner for a higher value of the Prandtl number, but the temperature distribution is quite interesting. With the increase of the Prandtl number, the wall heat flux becomes smaller with a flatter temperature near the wall and the temperature drops fast to the ambient temperature. A higher dropping slope is observed for a higher value of *Pr* in the fluid at a distance from the wall. Due to mass injection, the thermal penetration is much deeper than the mass suction cases.

Figures 12(a), 12(b) and 12(c) show the influence of mass transfer parameter on the temperature profiles. For a stretching problem, solutions exist for both mass suction and mass injection (Fig. 12-a). Under certain stretching strength and Prandtl number Pr, the wall heat flux reduces with increasing mass injection. The boundary layer thickness (thermal penetration) becomes thicker into the fluid. However for a shrinking sheet problem, solutions only exist for $s \geq \sqrt{-4\alpha}$. For both solution branches (Figs. 12-b and 12-c), the thermal boundary layer thickness and wall heat flux are quite similar. With the increase of mass suction, the temperature drops faster and the boundary layer becomes thinner for both branches. However, there are some crossovers among the temperature profiles under different mass suction for the lower solution branch, which does not occur for the upper solution branch.

The effects of wall stretching or shrinking strength are illustrated in Figs. 13 and 14. For the shrinking problem, both the upper solution (Fig. 13-a) and the lower solution (Fig. 13-b) show similar trend with boundary layer thicker for a high magnitude of shrinking strength. For the lower solution branches, some crossover points are observed for among certain temperature profiles. Quite different variation trends are observed for the stretching problem in Figs. 14(a) and (b). For both mass suction and mass injection, the boundary layers become thinner with the increase of stretching strength at the wall and the wall heat flux becomes higher.

The contour plot for $-\theta'(0)$ as a function of *s* and *Pr* are shown in Figs. 15(a) and (b) for $\alpha = 2$ and $\alpha = -2$, respectively. The results are consistent with the findings in the temperature profiles. For the stretching problem (Fig. 15-a) with mass suction at the wall, the heat flux increases with the increase of both *Pr* and *s*. But for mass injection, the variation trend becomes quite complicated under the effect of *Pr*. The heat flux still increases with the reduction of mass injection. For the Prandtl number under a certain mass injection, the heat flux first increases and then decreases with the increase of the Prandtl numbers. For the shrinking sheet problem, the variation trend is quite straightforward. As seen in Fig. 15(b), the wall heat flux increases with the increase of *Pr* and *s* for the lower solution branch. The results for the upper solution branch are very similar to the lower solution branch.

Some examples of the algebraically decaying temperature profiles are shown in Figs. 16(a) and (b). Under a certain shrinking strength, the boundary layer thickness becomes thinner for a higher value of *Pr*. With a certain *Pr* value, the boundary layers becomes thinner for a high magnitude of wall shrinking and the heat flux becomes higher. The wall heat flux as a function of *Pr* and α is straightforward as given in Eq. (45). The wall heat flux increases linearly with the increase of *Pr* and $\sqrt{-\alpha}$.

4. Conclusion

In this work, a general viscous fluid flow over a stretching/shrinking sheet was investigated. Exact solutions were obtained for the steady governing Navier-Stokes equations. The new solutions provide a more general formulation combining the stretching and shrinking wall problems as well as the asymptotic suction velocity profiles over a moving plate. The current results illustrate both exponentially and algebraically decaying solutions, multiple solution branches with infinite number of solutions for the flow field, and velocity overshoots. The energy equation ignoring viscous dissipation was solved exactly and the effects of the mass transfer parameter, the Prandtl number, and the wall stretching/shrinking strength on the temperature profiles and wall heat flux were also analyzed. The exact solution of this general flow configuration is a rare case for the Navier-Stokes equations and greatly enriches the understanding of the complicated nonlinear behavior.

References

[1] M.V. Karwe and Y. Jaluria, Numerical simulation of thermal transport associated with a continuous moving flat sheet in materials processing. ASME J. Heat Transfer 113 (1991) 612-619.

[2] L. J. Crane, Flow past a stretching plane. J. Appl. Math. Phys. (ZAMP) 21 (1970) 645-647.

[3] W.H.H. Banks, Similarity solutions of the boundary layer equations for a stretching wall. J. Mécan. Theoret. Appl. 2 (1983) 375-392.

[4] E. Magyari and B. Keller, Exact solutions for self-similar boundary-layer flows induced by permeable stretching surfaces. Eur. J. Mech. B-Fluids 19 (2000) 109-122.

[5] S. J. Liao and I. Pop, Explicit analytic solution for similarity boundary layer equations. Int. J. Heat Mass Transfer 47 (2004) 75-85.

[6] P. Carragher and L.J. Crane, Heat transfer on a continuous stretching sheet. J. Appl. Math. Mech. (ZAMM) 62 (1982) 564-565.

[7] J.L. Grubka and K.M. Bobba, Heat transfer characteristics of a continuous stretching surface with variable temperature. ASME J. Heat Transfer 107 (1985) 248-250.

[8] B.K. Dutta, P. Roy and A.S. Gupta, Temperature field in flow over a stretching sheet with uniform heat flux. Int. Comm. Heat Mass Transfer 12 (1985) 89-94.

[9] P.S. Gupta and A.S. Gupta, Heat and mass transfer on a stretching sheet with suction or blowing. Canad. J. Chem. Engng. 55 (1977) 744-746.

[10] R.C. Bataller, Similarity solutions for flow and heat transfer of a quiescent fluid over a nonlinearly stretching surface. J. Mater. Processing Techn. 203 (2008) 176-183.

[11] E. Magyari and P.D. Weidman, Heat transfer on a plate beneath an external uniform shear flow. Int. J. Thermal Sci. 45 (2006) 110-115.

[12] G.E. Cossali, Similarity solutions of energy and momentum boundary layer equations for a power-law shear driven flow over a semi-infinite flat plate. Eur. J. Mech. B/Fluids 25 (2006) 18-32.

[13] T. Fang, Flow and heat transfer characteristics of the boundary layers over a stretching surface with a uniform-shear free stream. Int. J. Heat Mass Transfer 51 (2008) 2199-2213.

[14] E. Magyari and B. Keller, Heat transfer characteristics of boundary-layer flows induced by continuous surfaces stretched with prescribed skin friction. Heat Mass Transfer 42 (2006) 679-687.

[15] H.I. Andersson, Slip flow past a stretching surface. Acta Mech. 158 (2002) 121-125.

[16] A. Chakrabarti and A.S. Gupta, Hydromagnetic flow and heat transfer over a stretching sheet. Quart. Appl. Math. 37 (1979) 73-78.

[17] I. Pop and T.Y. Na, A note on MHD flow over a stretching permeable surface. Mech. Res. Commun. 25 (1998) 263-269.

[18] H.I. Andersson, K.H. Bach and B.S. Dandapat, Magnetohydrodynamic flow of a power-law fluid over a stretching sheet. Int. J. Non-Linear Mech. 29 (1992) 929-936.

[19] A. Pantokratoras, Flow adjacent to a stretching permeable sheet in a Darcy-Brinkman porous medium. Transport Porous Media 80 (2009) 223-227.

[20] C.Y. Wang, The three-dimensional flow due to a stretching flat surface. Phys. Fluids 27 (1984) 1915-1917.

[21] N. Afzal, A. Badaruddin and A.A. Elgarvi, Momentum and transport on a continuous flat surface moving in a parallel stream. Int. J. Heat Mass Transfer 36 (1993) 3399–3403.

[22] N. Afzal, Momentum transfer on power law stretching plate with free stream pressure gradient. Int. J. Engng. Sci. 41 (2003) 1197-1207.

[23] P.D. Weidman, D.G. Kubitschek and A.M.J. Davis AMJ (2006) The effect of transpiration on self-similar boundary layer flow over moving surfaces. Int. J. Engng. Sci. 44 (2006) 730–737.

[24] A. Ishak, R. Nazar and I. Pop, Flow and heat transfer characteristics on a moving flat plate in a parallel stream with constant surface heat flux. Heat Mass Transfer 45 (2009) 563-567.

[25] M. Miklavčič and C.Y. Wang, Viscous flow due to a shrinking sheet. Quart. Appl. Math. 46 (2006) 283-290.

[26] S. Goldstein, On backward boundary layers and flow in converging passages. Journal of Fluid Mechanics 21 (1965) 33-45.

[27] T. Fang, Boundary layer flow over a shrinking sheet with power-law velocity. Int. J. Heat Mass Transfer 51 (2008) 5838-5843.

[28] T. Fang, W. Liang and C.F. Lee, A new solution branch for the Blasius equation - A shrinking sheet problem. Comp. & Math. with Appl. 56 (2008) 3088-3095.

[29] T. Fang and J. Zhang, Closed-form exact solutions of MHD viscous flow over a shrinking sheet. Comm. Nonlinear Sci. Numer. Simul. 14 (2009) 2853-2857.

[30] T. Fang, J. Zhang and S. Yao, Viscous flow over an unsteady shrinking sheet with mass transfer. Chin. Phys. Lett. 26 (2009) 014703.

[31] T. Fang, J. Zhang and S. Yao, Slip MHD viscous flow over a stretching sheet- an exact solution. Commun. Nonlinear Sci. Numer. Simulat. 14 (2009) 3731-737.

[34] C.Y. Wang, Stagnation flow towards a shrinking sheet. Int. J. Non-Linear Mech. 43 (2008) 377-382.

[32] T. Hayat, Z. Abbas, T. Javed and M. Sajud, Three-dimensional rotating flow induced by a shrinking sheet for suction. Chaos, Solitons and Fractals 39 (2009) 1615-1626.

[33] Y.Y. Lok, A. Ishak and I. Pop, MHD stagnation-point flow towards a shrinking sheet (submitted).

[35] T. Fang, J. Zhang, Heat transfer over a shrinking sheet- An analytical solution, Acta Mechanica, DOI: 10.1007/s00707-009-0183-2, 2009, in press

CAPTIONS OF FIGURES

Fig. 1 The solution domain β of at different values of α as a function of the mass transfer parameter

Fig. 2 Velocity profiles of the upper solution branch (a) and the lower solution branch (b) at $s = 4$ under different negative values of α

Fig. 3 Velocity profiles of different positive values of α under mass suction (a) and mass injection (b)

Fig. 4 Some typical dimensionless streamlines of the two solution branches for the shrinking sheet problem under different combinations of control parameters

Fig. 5 Some typical dimensionless streamlines of the stretching sheet problem for different combinations of control parameters under mass suction (a-b) and mass injection (c-d)

Fig. 6 Profiles of $f'(\eta)$ (a) and $f(\eta)$ (b) for the algebraically decaying solutions under different values of α

Fig. 7 Profiles of $g(\eta)$ for the algebraically decaying solutions under different values of α (a) and positive C_1 (b)

Fig. 8 Profiles of $g(\eta)$ for the algebraically decaying solutions under different values of α (a) and negative C_1 (b)

Fig. 9 Some examples of non-dimensional streamlines for the algebraically decaying solution under positive C/a (a) and negative C/a (b)

Fig. 10 Temperature profiles of the upper solution branch (a) and the lower solution branch (b) for a shrinking sheet problem under different values of *Pr*

Fig. 11 Temperature profiles of a stretching sheet problem under mass suction (a) and mass injection (b) for different values of *Pr*

Fig. 12 Effects of mass transfer parameter on the temperature profiles: (a) stretching sheet, (b) upper solution of a shrinking sheet, and (c) lower solution of a shrinking sheet

Fig. 13 Effects of wall shrinking strength on the temperature profiles: (a) upper solution branch and (b) lower solution branch

Fig. 14 Effects of wall stretching strength on the temperature profiles: (a) mass suction and (b) mass injection

Fig. 15 Contour plots of $-\theta'(0)$ as a function of *Pr* and *s* for the stretching sheet problem (a) and the lower solution branch of the shrinking sheet problem

Fig. 16 Effects of the Prandtl number (a) and wall shrinking strength (b) on the temperature profiles of the algebraically decaying solution

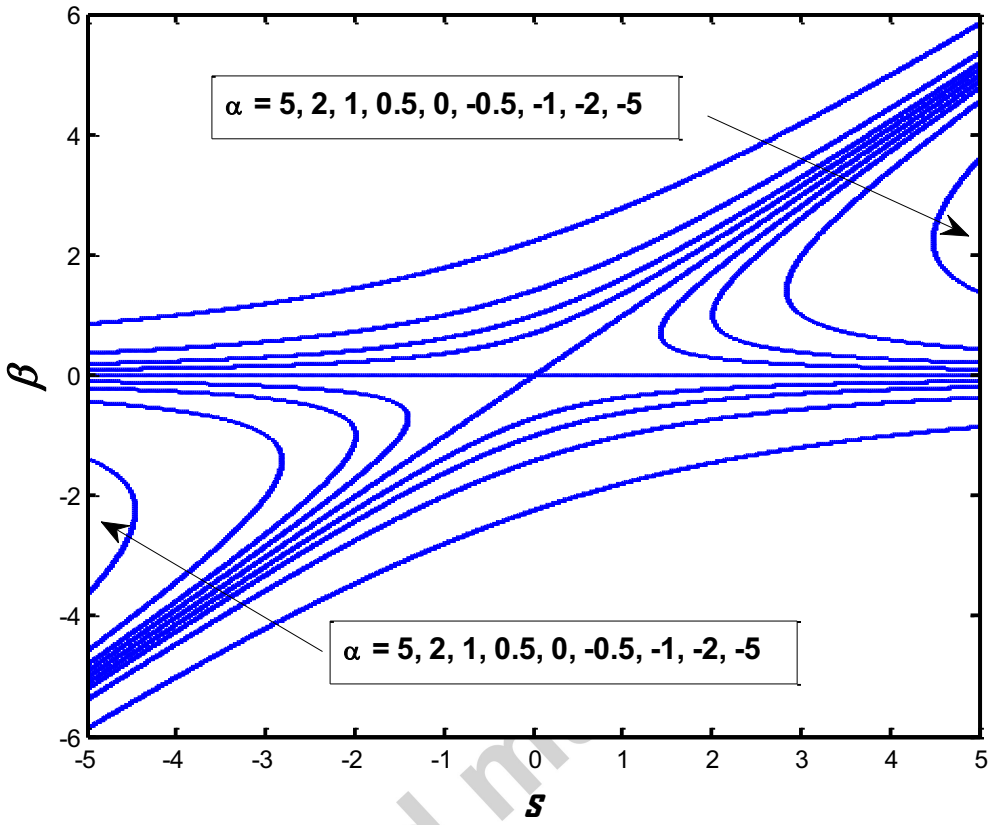

Fig. 1 The solution domain for β at different values of α as a function of the mass suction parameter, s

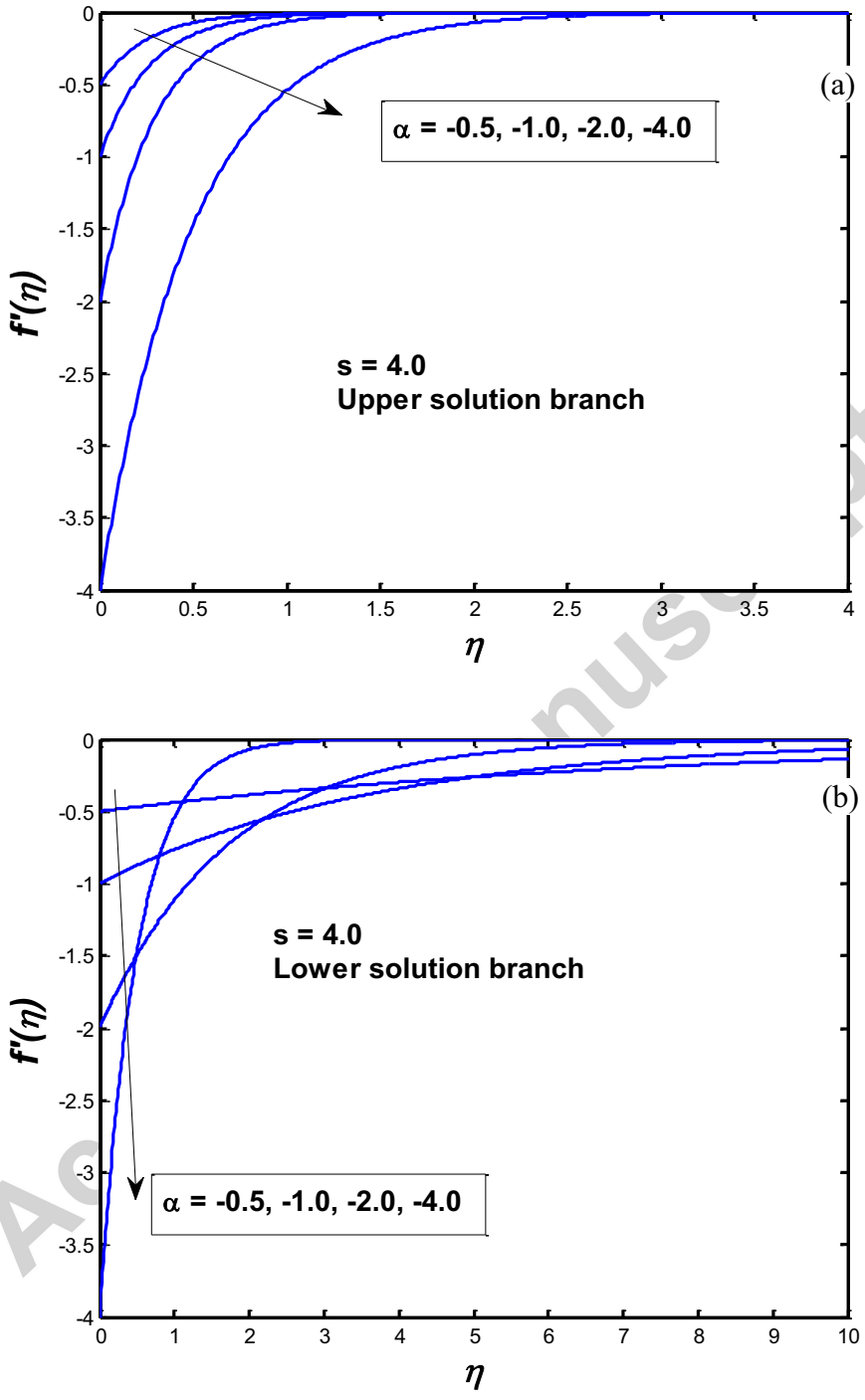

Fig. 2 Velocity profiles of the upper solution branch (a) and the lower solution branch (b) at $s = 4$ under different negative values of α

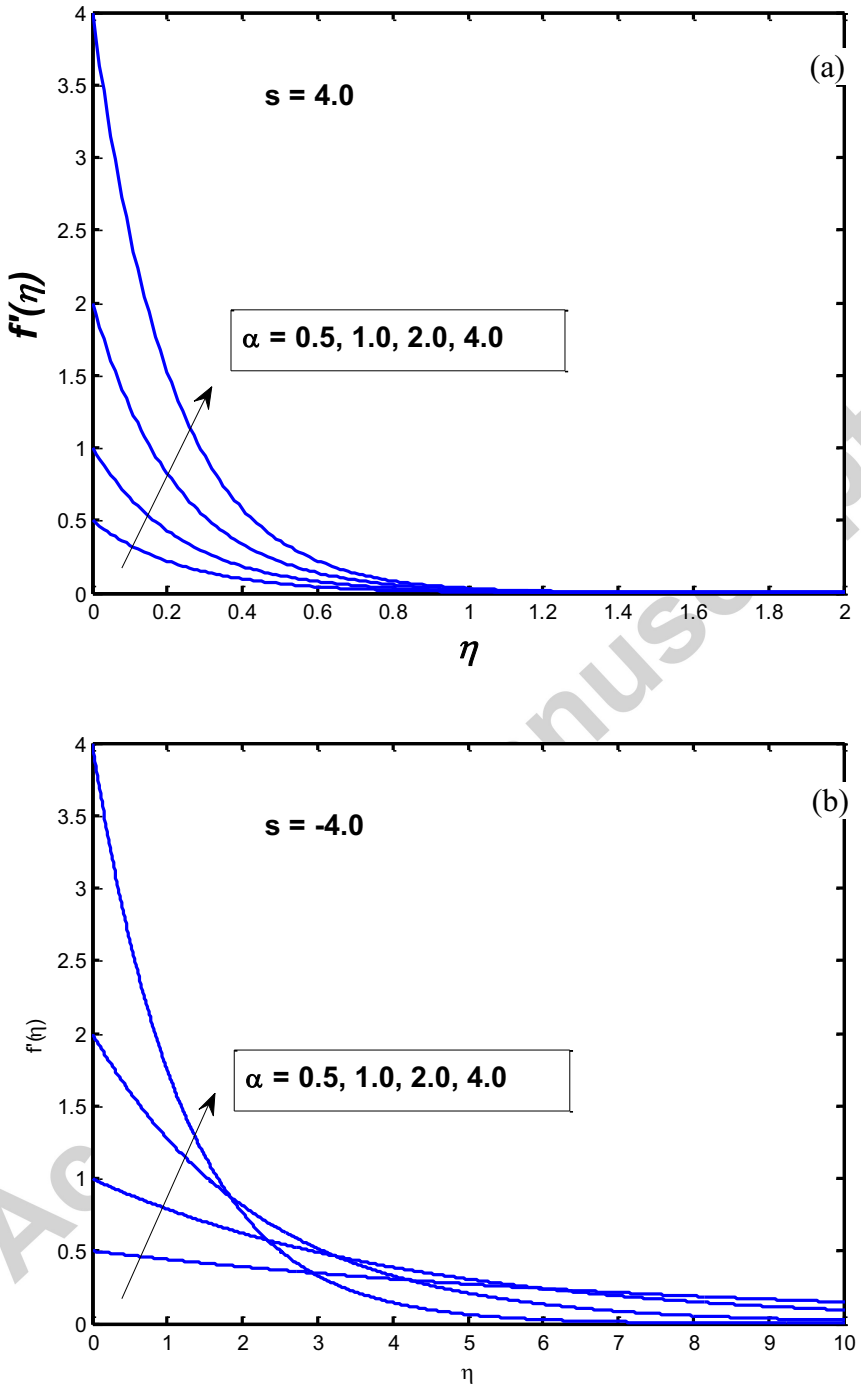

Fig. 3 Velocity profiles of different positive values of α under mass suction (a) and mass injection (b)

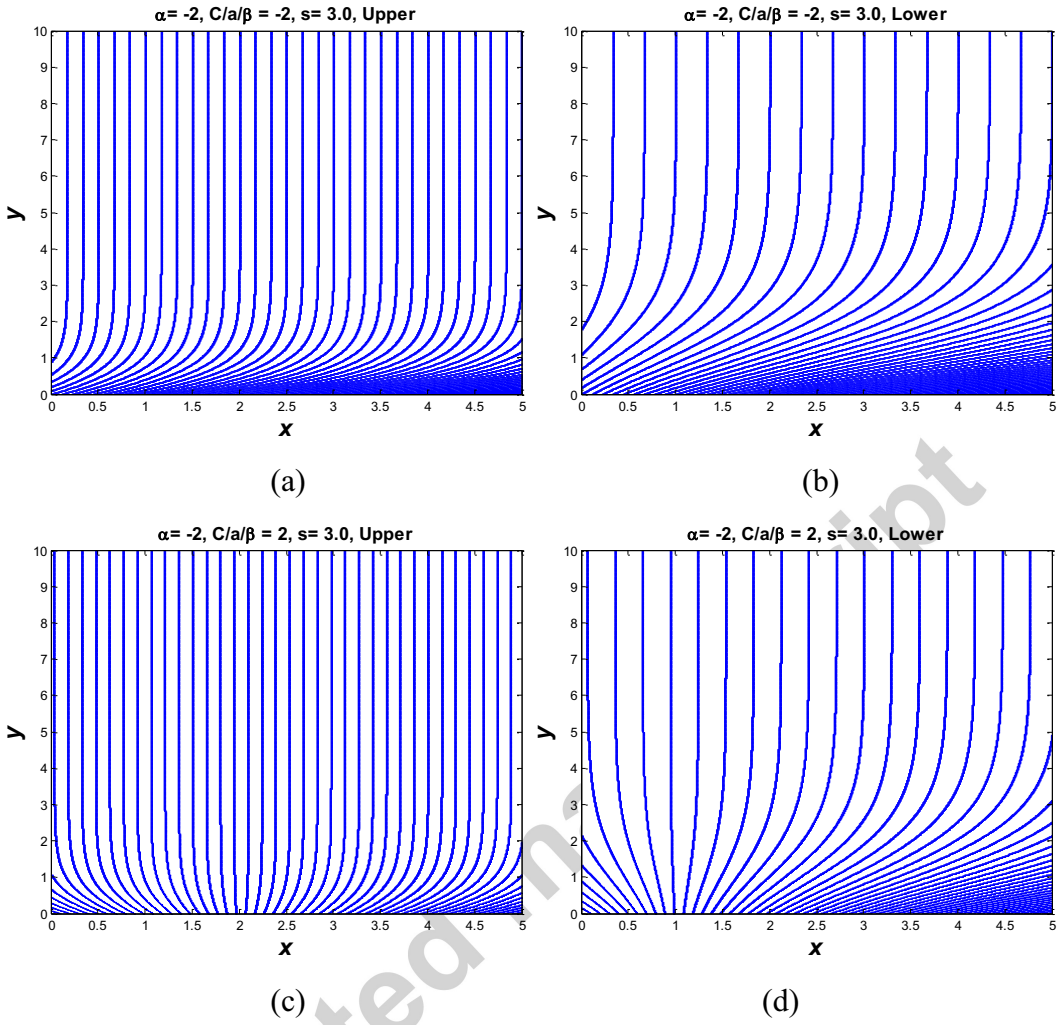

Fig. 4 Some typical dimensionless streamlines of the two solution branches for the shrinking sheet problem under different combinations of control parameters

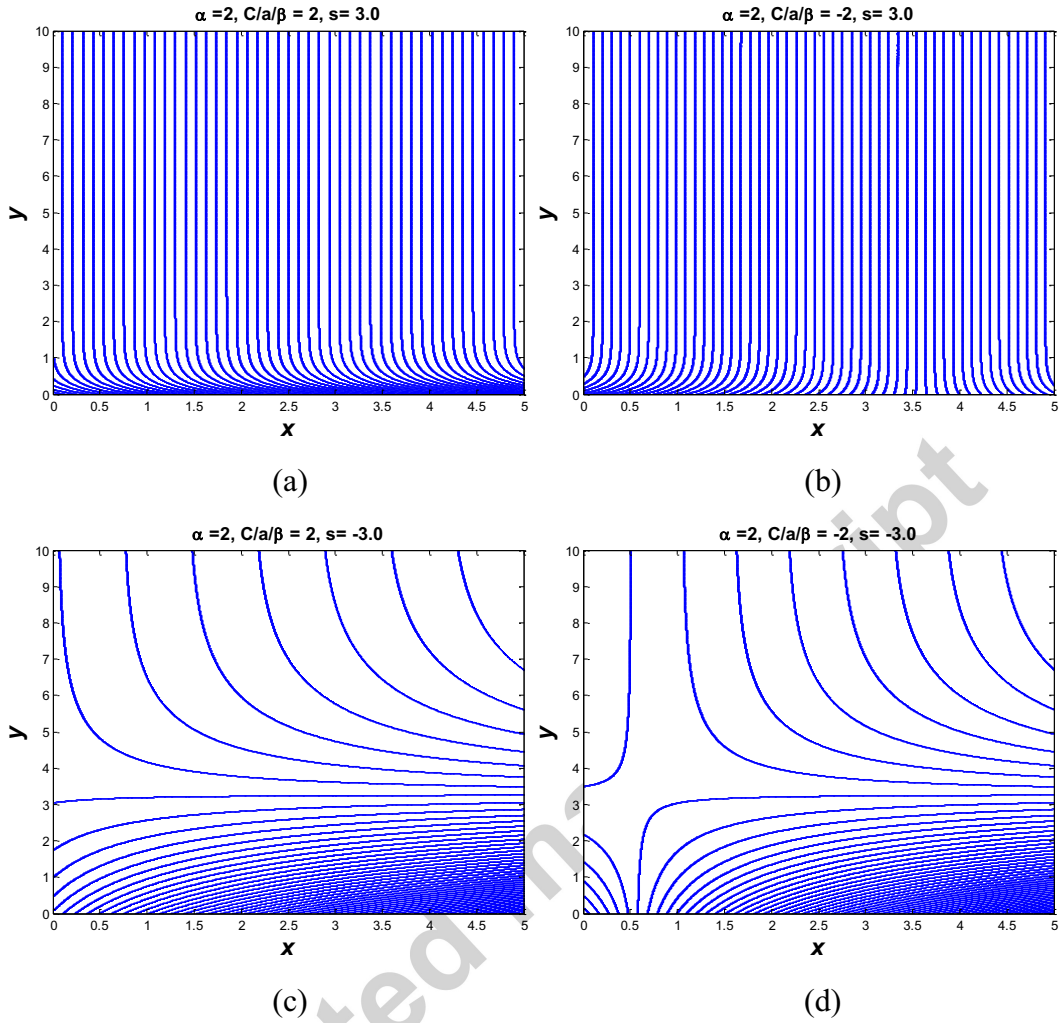

Fig. 5 Some typical dimensionless streamlines of the stretching sheet problem for different combinations of control parameters under mass suction (a-b) and mass injection (c-d)

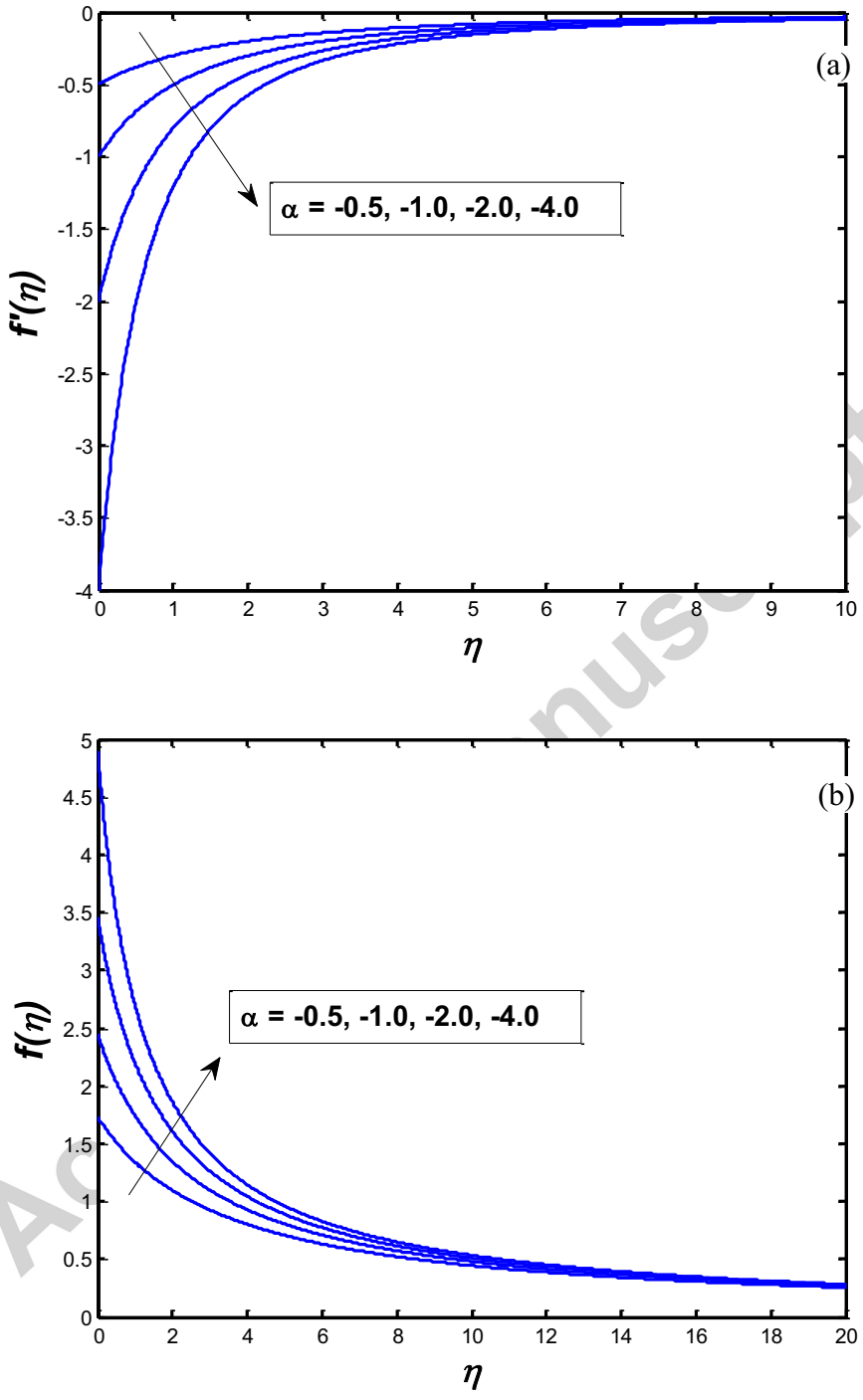

Fig. 6 Profiles of $f'(\eta)$ (a) and $f(\eta)$ (b) for the algebraically decaying solutions under different values of α

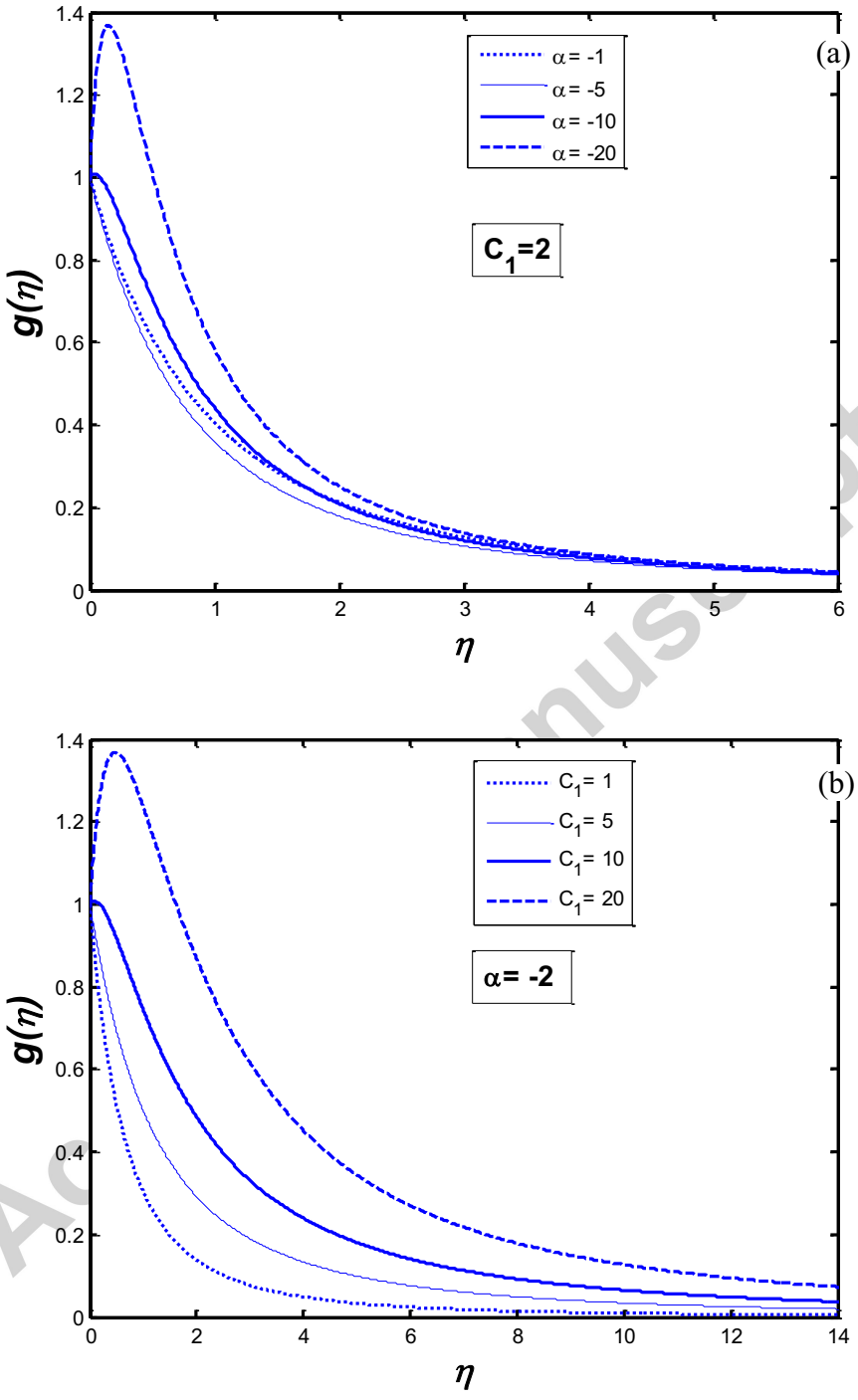

Fig. 7 Profiles of $g(\eta)$ for the algebraically decaying solutions under different values of α (a) and positive C_1 (b)

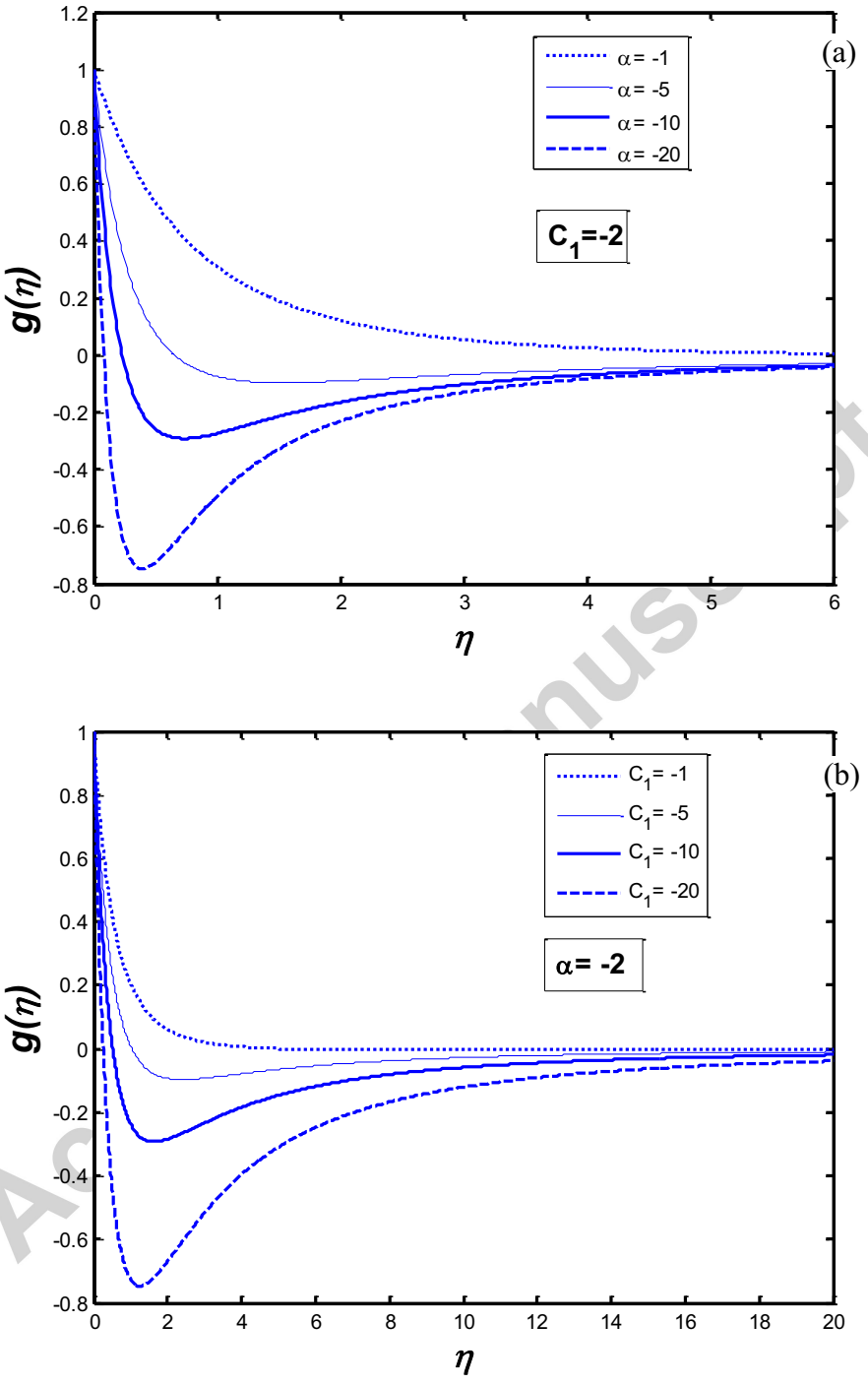

Fig. 8 Profiles of $g(\eta)$ for the algebraically decaying solutions under different values of α (a) and negative C_1 (b)

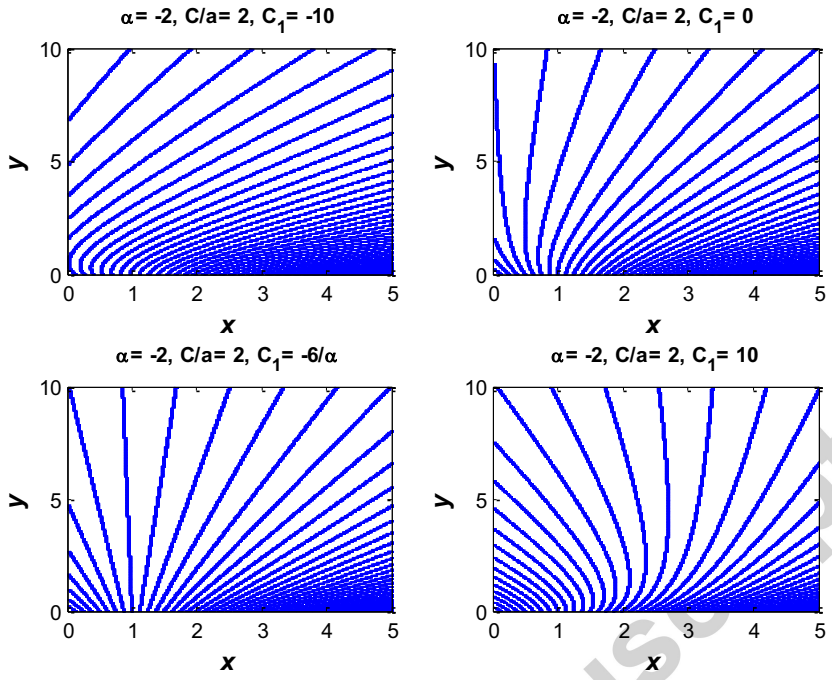

(a)

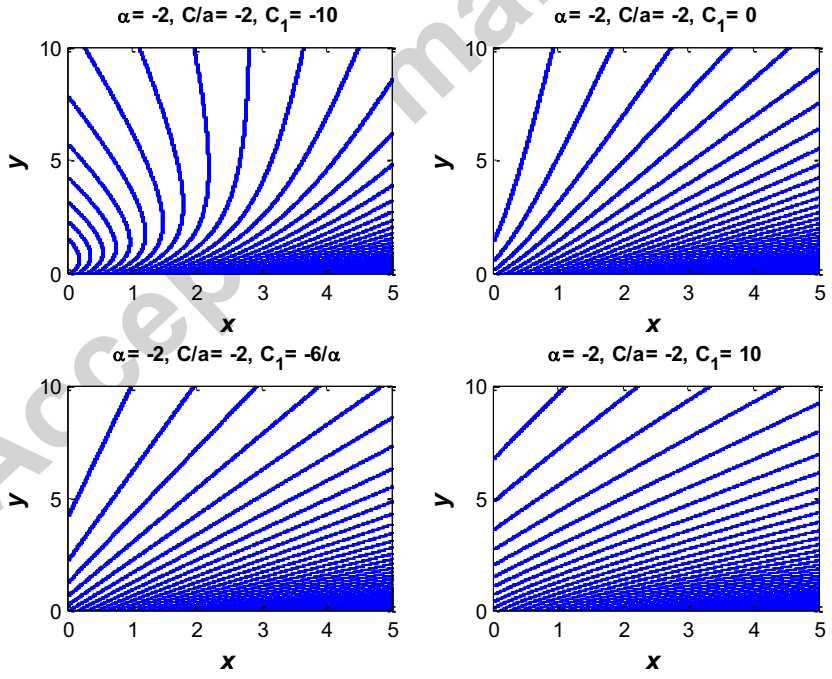

(b)

Fig. 9 Some examples of non-dimensional streamlines for the algebraically decaying solution under positive C/a (a) and negative C/a (b)

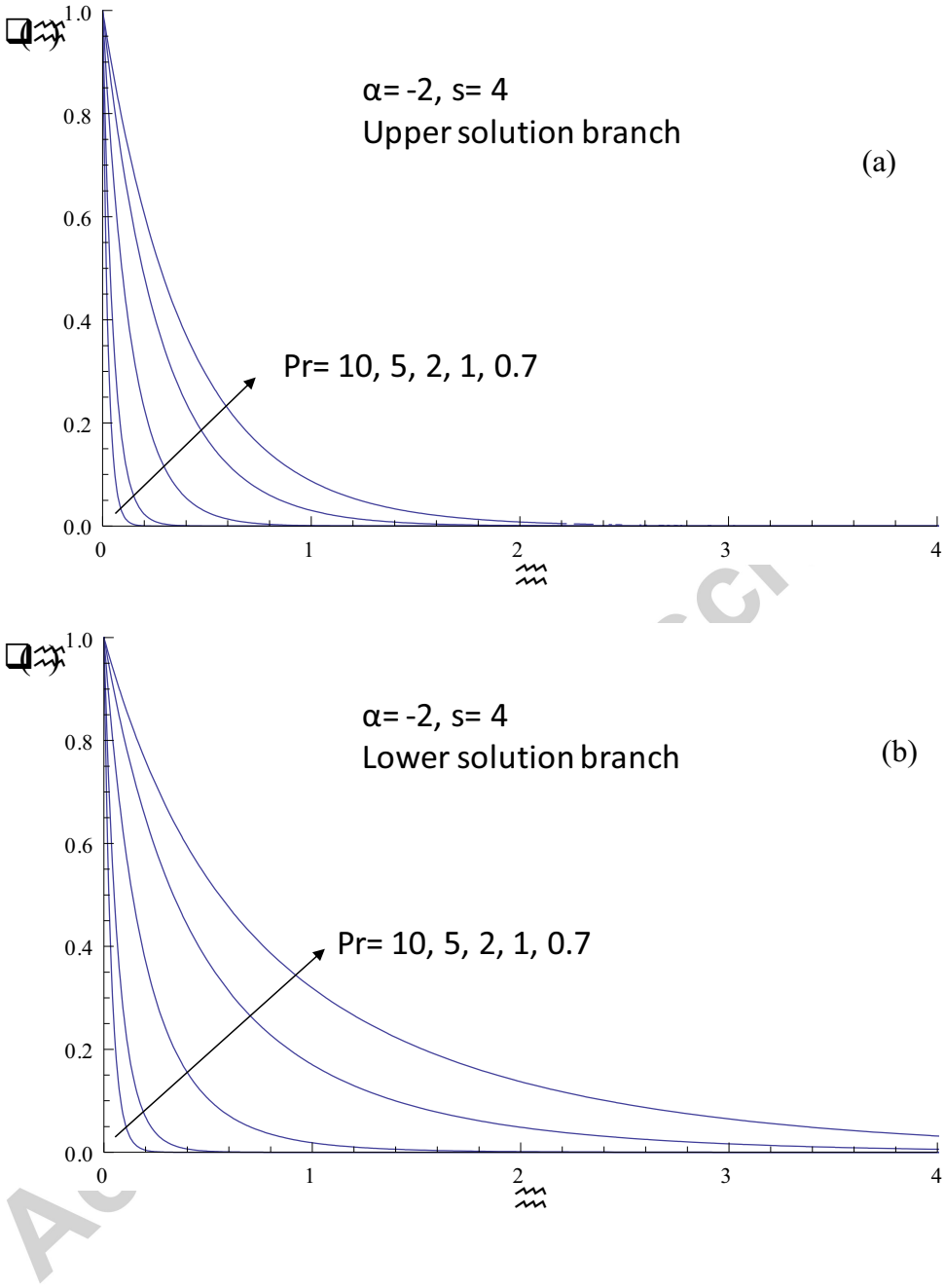

Fig. 10 Temperature profiles of the upper solution branch (a) and the lower solution branch (b) for a shrinking sheet problem under different values of *Pr*

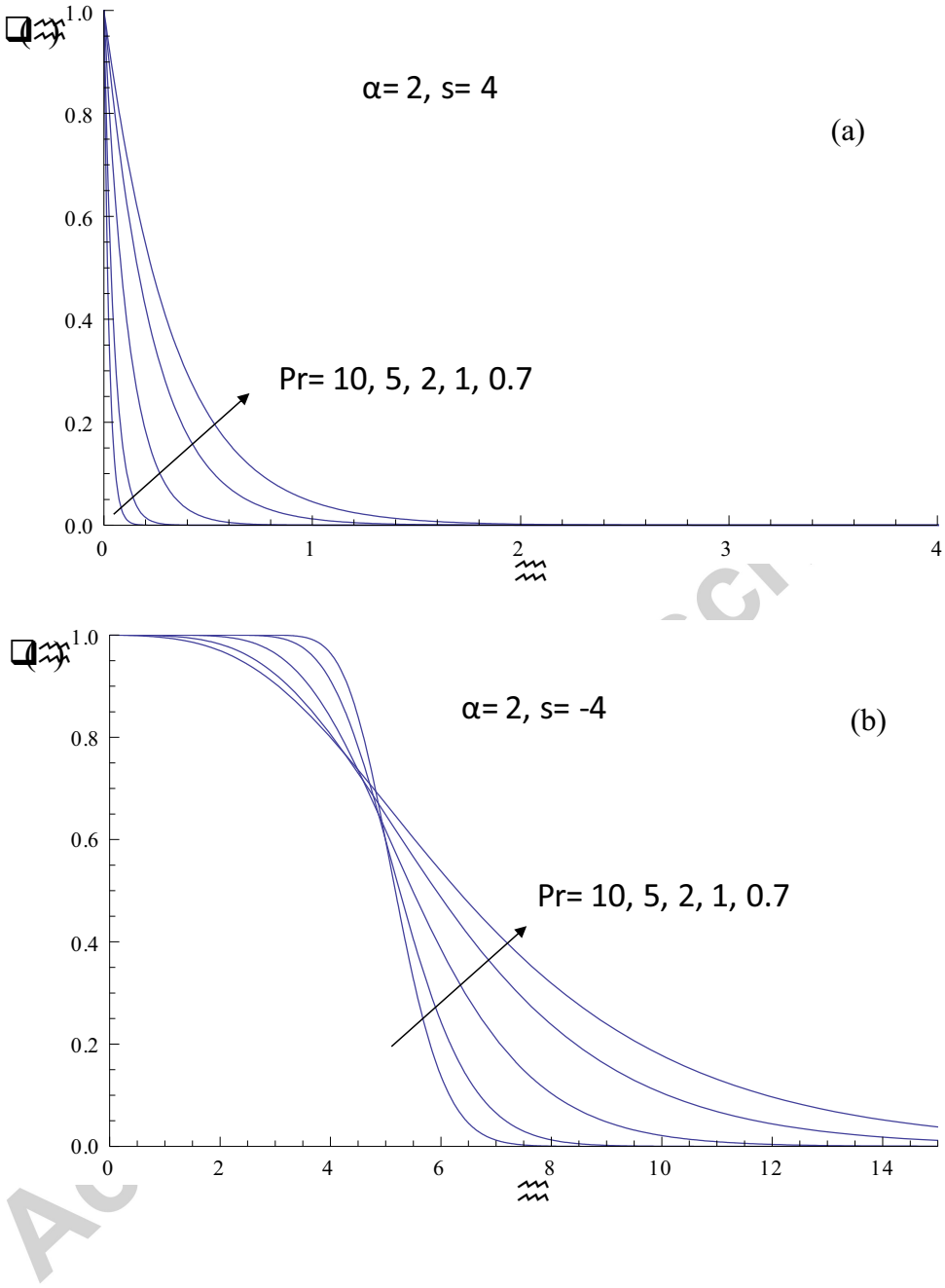

Fig. 11 Temperature profiles of a stretching sheet problem under mass suction (a) and mass injection (b) for different values of *Pr*

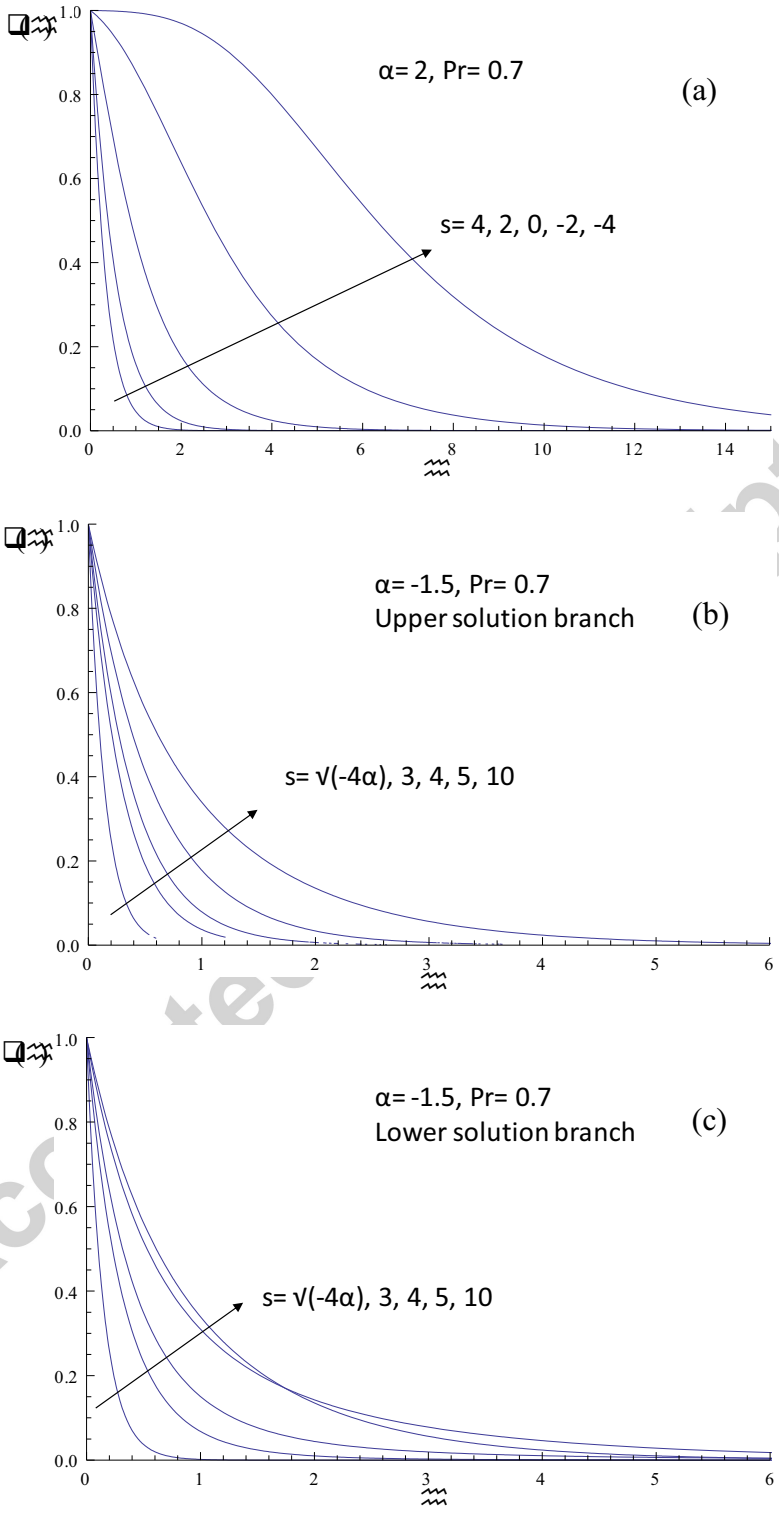

Fig. 12 Effects of mass transfer parameter on the temperature profiles: (a) stretching sheet, (b) upper solution of a shrinking sheet, and (c) lower solution of a shrinking sheet

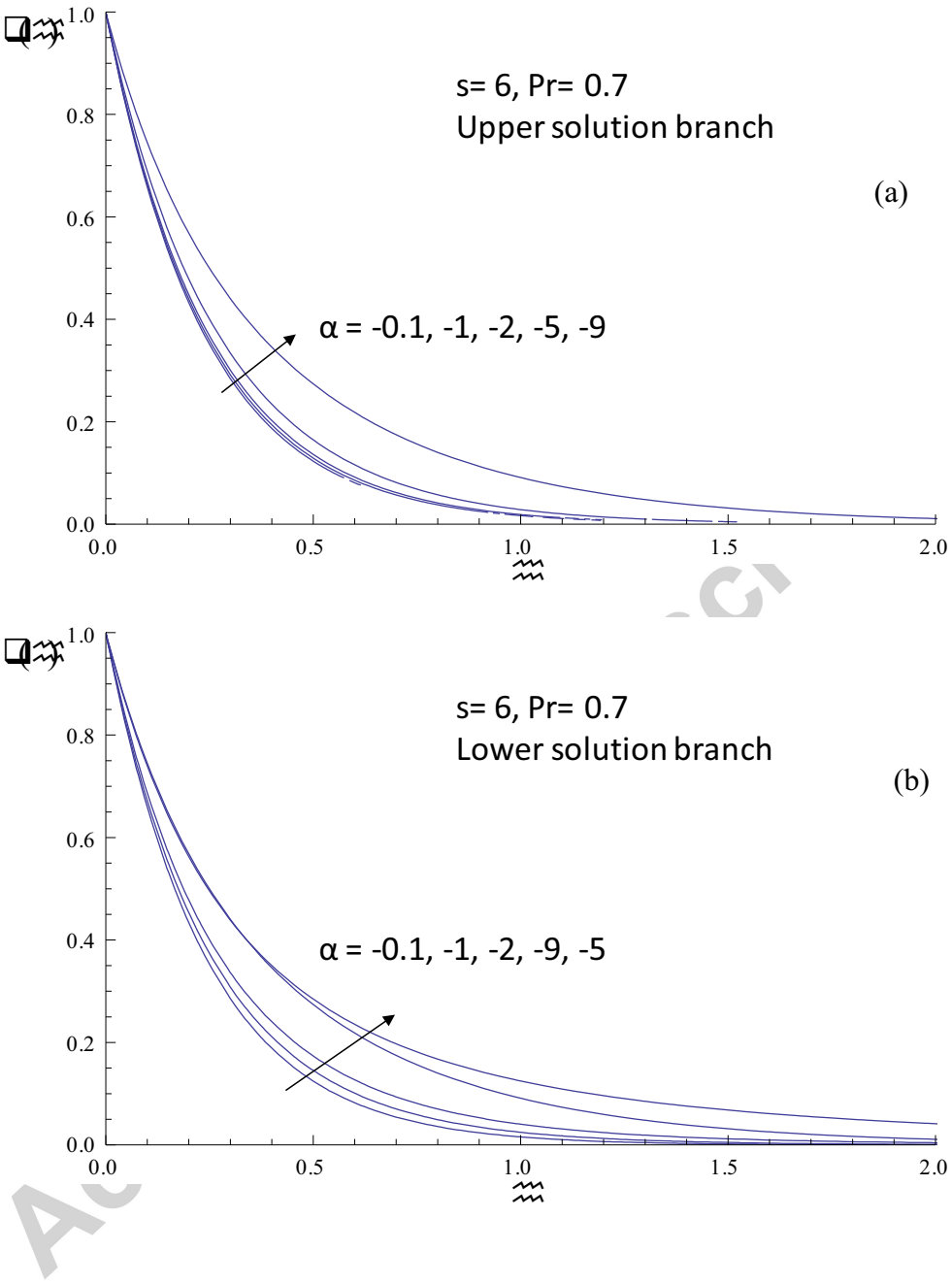

Fig. 13 Effects of wall shrinking strength on the temperature profiles: (a) upper solution branch and (b) lower solution branch

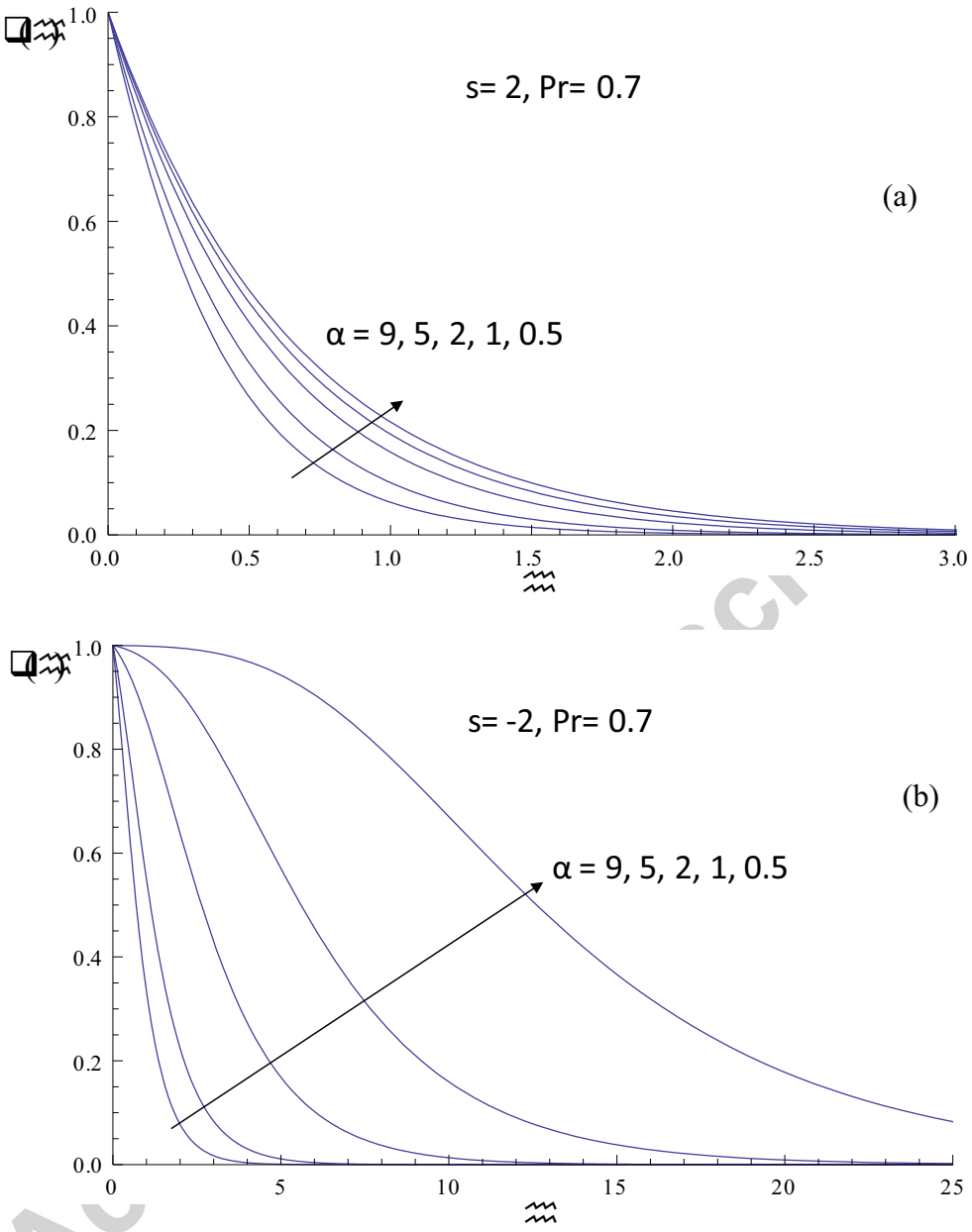

Fig. 14 Effects of wall stretching strength on the temperature profiles: (a) mass suction and (b) mass injection

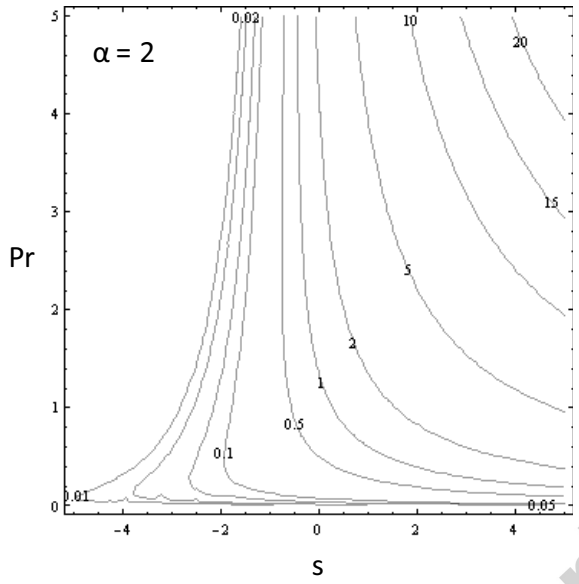

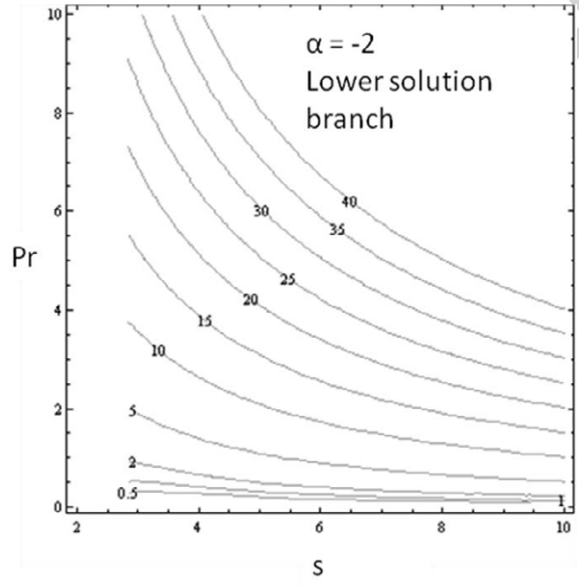

(a) (b)

Fig. 15 Contour plots of $-\theta'(0)$ as a function of *Pr* and *s* for the stretching sheet problem (a) and the lower solution branch of the shrinking sheet problem

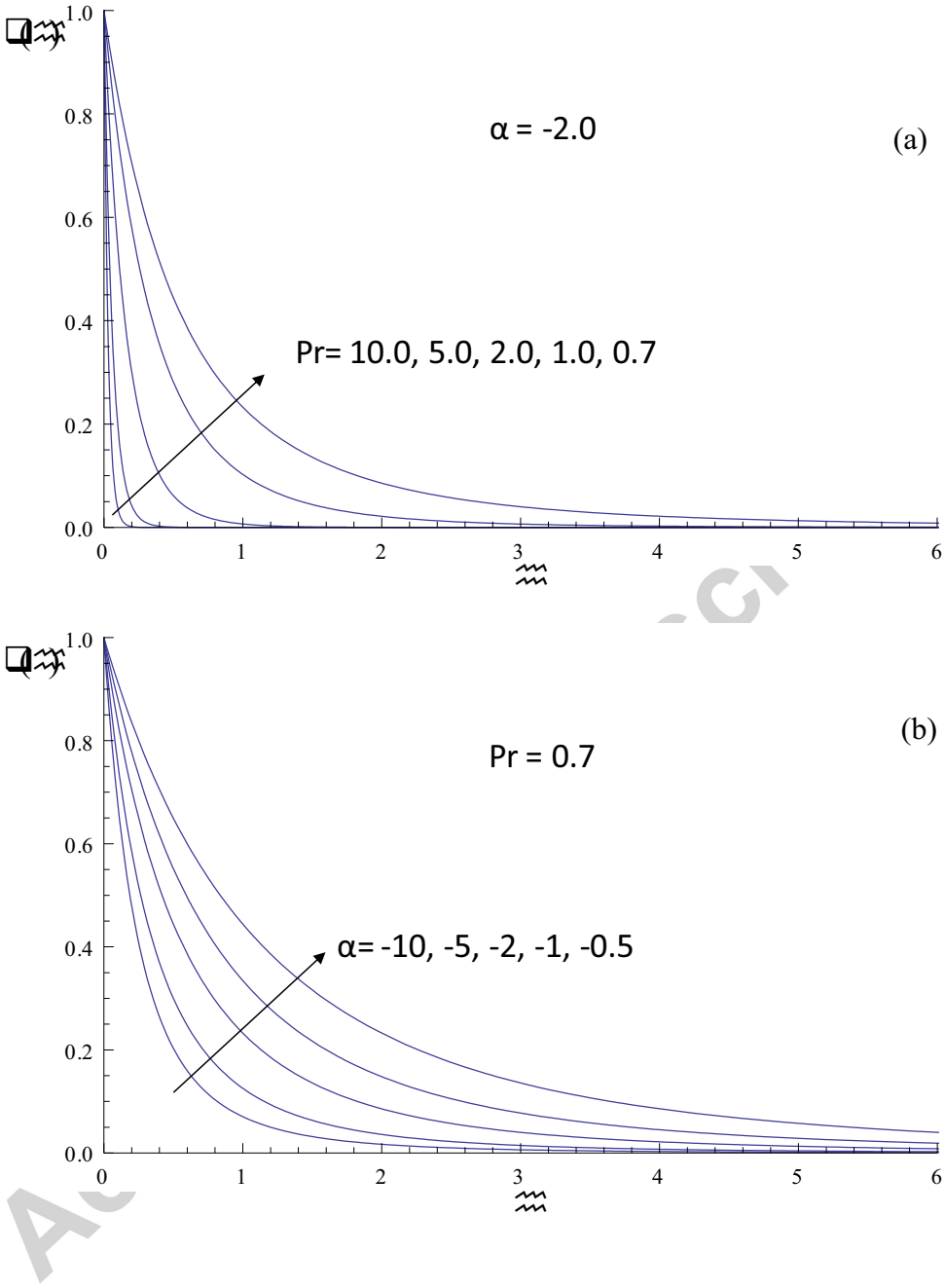

Fig. 16 Effects of the Prandtl number (a) and wall shrinking strength (b) on the temperature profiles of the algebraically decaying solution

- Momentum and heat transfer of flow over a stretching/shrinking sheet are investigated
- Exact solutions of the Navier-Stokes equations are found
- Both exponentially and algebraically decaying solutions are observed
- Multiple solutions with infinite number of solutions for the flow field are obtained